Periodic Bicontinuous Structures Formed on the Top Surface of Asymmetric Triblock Terpolymer Thick Films

Karim Aissou, Muhammad Mumtaz, Nils Demazy, Gilles Pécastaings, Guillaume Fleury, Georges Hadziioannou

Periodic Bicontinuous Structures Formed on the Top Surface of Asymmetric Triblock Terpolymer Thick Films

Karim Aissou,[1*] Muhammad Mumtaz,[2] Nils Demazy,[2] Gilles Pécastaings,[2] Guillaume Fleury,[2] and Georges Hadziioannou[2]

[1]Institut Européen des Membranes, Université de Montpellier - CNRS - ENSCM, 300 Avenue du Professeur Emile Jeanbrau, F-34090 Montpellier, France

[2]Laboratoire de Chimie des Polymères Organiques, Univ. Bordeaux, CNRS, Bordeaux INP, LCPO, UMR 5629, F-33600, Pessac, France

E-mail: karim.aissou@umontpellier.fr

Abstract: The combination of the non-solvent induced phase separation (NIPS) process with a solvent vapor annealing (SVA) treatment is used to produce asymmetric and hydrophobic thick films having different long-range ordered network nanostructures, which are inaccessible *via* currently available membrane fabrication methods. We show that the disordered phase generated by NIPS on the material top surface can be transformed into a highly-ordered bicontinuous network nanostructure during the SVA process without disrupting the substructure morphology. For instance, by using a straightforward blending approach, either a triply periodic alternating diamond (D^A) structure or a core-shell perforated lamellar (PL) phase were demonstrated on the skin layer of fully hydrophobic poly(1,1-dimethyl silacyclobutane)-*block*-polystyrene-*block*-poly(methyl methacrylate) (PDMSB-*b*-PS-*b*-PMMA) thick films. Such material fabrication method, enabling the formation of a sponge-like substructure topped by a network phase having an excellent long-range order, provides an appealing strategy to facilitate the manufacture of next-generation membranes at large scale since these bicontinuous morphologies obviate the need of the nanochannel alignment.

Keywords: Solvent vapor annealing, ABC triblock terpolymer, self-assembly, asymmetric thick film, phase inversion process.

Asymmetric and isoporous block copolymer (BCP) membranes are promising materials to achieve a better figure of merit compared to the state of the art membranes as their unique architecture allows overcoming the ubiquitous permeability-selectivity trade-off.[1–4] To produce such kind of high-performance materials, Peinemann *et al*.[5] have used an elegant approach which combines the self-assembly of BCPs into an out-of-plane cylindrical

nanostructure on the material top surface with the formation of a macroporous substructure generated by non-solvent induced phase separation (NIPS). However, a perfect-control of the nanopore formation is challenging to achieve with the SNIPS method (*i.e.*, Self-assembly + NIPS) due to the fact that, at best, a kinetically trapped morphology derived from a micellization process is formed on the material skin layer when appropriate manufacturing conditions can be defined.[6–8] Indeed, the complex exchange/migration of the non-solvent occurring during the porosity formation makes that isoporous membranes with pores extending over the top separation layer were solely demonstrated for specific amphiphilic AB- and ABC-type BCP systems since the hydrophilic block plays a crucial role in creating pores during the precipitation process.[9–14]

To produce innovative membranes with smart nanopores (*e.g.*, thermo-, ion and/or pH-responsive channels),[15–18] a large panoply of chemically distinct amphiphilic BCP materials has been generated by SNIPS. In addition, the self-assembly of blends of two chemically interacting amphiphilic BCPs was revealed to be a powerful strategy to achieve highly porous membranes with pore diameters as small as 1.5 nm.[19] However, so far, only few of these chemically distinct amphiphilic BCP membranes exhibit a dense top surface with long-range ordered nanopores.

The more challenging fabrication of fully hydrophobic BCP materials with an asymmetric structure or ordered pores over the whole film has been recently demonstrated by SNIPS[20] or a strategy related to SNIPS,[21] respectively. For the asymmetric material, although a complete pore formation was evidenced on the top layer during the SNIPS process, the resulting BCP morphology was arranged into a short-range ordered array with a broad pore size distribution, limiting the selectivity of the top separation layer.[20]

In this work, we efficiently combine the NIPS process and the solvent vapor annealing (SVA) approach to demonstrate that fully hydrophobic triblock terpolymer thick films can

also be manufactured with a sponge-like morphology topped by a long-range ordered nanostructure. We show that no-effort are required to pre-order the poly(1,1-dimethyl silacyclobutane)-*block*-polystyrene-*block*-poly(methyl methacrylate) (PDMSB-*b*-PS-*b*-PMMA) terpolymers on the material top surface during the NIPS process since the SVA treatment transforms the kinetically trapped poorly-ordered phase into a well-defined nanostructure. To obviate the need of alignment of the BCP nanodomains, we show that different network structures such as the alternating diamond (D^A) and perforated-lamellar (PL) phases can be readily produced on the top surface layer by using a simple blending strategy. As all the material architectures, consisting of a sponge-like substructure topped by a network structure having a high-areal density of well-defined continuous nanopathways, are highly-desired for the next generation-membranes, the NIPS-SVA process could be envisioned as a promising methodology towards the reproducible manufacturing in large scale of asymmetric and isoporous BCP membranes.

Results

The PDMSB-*b*-PS-*b*-PMMA used in this work was prepared by a sequential anionic polymerization, as described previously,[22] to achieve a perfect control of the molecular weight, $M_{n,}$ (34 kg.mol^{-1}) with a narrow dispersity ($Đ$ = 1.11) and a symmetric volume composition, Φ, (Φ_{PDMSB} = 0.32, Φ_{PS} = 0.36, Φ_{PMMA} = 0.32). This triblock terpolymer is non-frustrated[23] since the Flory–Huggins interaction parameter, $\chi_{PDMSB\text{-}PMMA}$, between the two end blocks (*i.e.*, PDMSB and PMMA) is higher than the other pairs, $\chi_{PDMSB\text{-}PS}$ and $\chi_{PS\text{-}PMMA}$ ($\chi_{PS\text{-}PMMA} \approx 0.04 < \chi_{PDMSB\text{-}PS} \approx 0.07 < \chi_{PDMSB\text{-}PMMA} \approx 0.2$).[22,24] Note that both (spin-coated) thin films and (drawn) asymmetric thick films made of this non-frustrated terpolymer exhibit a 39 nm period core-shell cylindrical structure having an in-plane orientation (*i.e.*, an undesirable

nanodomain orientation) when exposed to a chloroform ($CHCl_3$) vapor (see **Fig. S1**).[21] A preferential swelling of the PDMDB domains under a $CHCl_3$ stream makes that core-shell cylindrical structure differs from the bulk morphology since the SAXS profile of the thermally-annealed (24h, 180°C) PDMSB-*b*-PS-*b*-PMMA sample shows a first-order peak, q^*, at 0.173 nm^{-1} and higher order peaks located at q/q^* = 1, 2, 3, 4, 5, 6, 7, and 8, consistent with a lamellar phase having a period of ~36.3 nm (see **Fig. S2**).

To alleviate the need for domain alignment, different highly-ordered network structures were produced on the top surface layer by blending the PDMSB-*b*-PS-*b*-PMMA thick films with either 25 wt. % or 35 wt. % of PDMSB-*b*-PS chains (Φ_{PDMSB} = 0.29, M_n = 21.6 $kg.mol^{-1}$ and $Đ$ = 1.09). Importantly, blends of this triblock terpolymer with different amounts of a small PS homopolymer (hPS, 3 $kg.mol^{-1}$) gave access to well-ordered cylindrical or spherical nanodomains on a denser sponge-like substructure. Here, the possible miscibility of PMMA domains with the small hPS chains, due to the low $\chi_{PS\text{-}PMMA}$ value, should be taken into account to explain the different phase behaviors of such blends.

Blended PDMSB-*b*-PS-*b*-PMMA thick films were drawn into a silicon substrate from a 18 % wt. polymer solution in a di-solvent mixture of 1,4-dioxane and tetrahydrofuran (DOX/THF: 80/20 by weight) using a doctor's blade set at a gate height of 225 μm. After the thick film was casted, the di-solvent mixture was allowed to evaporate for 15s to form a dense top surface layer. The blended PDMSB-*b*-PS-*b*-PMMA thick films were then plunged in a water bath in order to induce the formation of a sponge-like substructure by NIPS. Note that a fluorine-rich reactive ion etching (RIE) plasma was performed to partially and preferentially remove PDMSB and PMMA domains, respectively, prior to take scanning electronic microcopy (SEM) images (plasma conditions are: 40 W, 17 sccm CF_4 and 3 sccm O_2, 180 mTorr, 45 s).

The SEM image presented in **Figure 1a** shows the resulting top surface morphology of a blended (25% wt.) PDMSB-*b*-PS-*b*-PMMA thick film generated by NIPS for a solvent evaporation time of 15s. In such conditions, the material top layer consists of dense regions formed by collapsed micelles (gray) which coexist with sub-100 nm diameter pores (black) randomly distributed across the surface. Conversely, a highly-ordered hexagonal nanoring-like array with a period of 38.5 nm is produced when the thick film is afterwards exposed to a $CHCl_3$ vapor during 3h (see **Fig. 1b**). This nanoring-like array pattern is consistent with the characteristic (111) crystallographic plane of an alternating diamond (D^A, space group $Fd\bar{3}m$) structure oriented parallel to the air surface since it qualitatively resembles to the simulated cross-sectional view cut parallel to the D^A (111) plane (see **Fig. 1b** inset) and to the D^A (111) pattern recently observed in bulk from binary blends of polyisoprene-*b*-PS-*b*-poly(2-vinyl pyridine) (PI-*b*-PS-*b*-P2VP).[26] The presence of the D^A (210) pattern as shown in **Figure 1c** further confirms the formation of a D^A structure, which consists of two chemically distinct (PDMSB and PMMA) and mutually interwoven networks embedded in a PS matrix (see **Fig. S3**). The D^A (210) pattern presents wavy stripes ordered into a rectangular array with the lattice parameters a = 45 nm and b = 21 nm. The ratio a/b equal to 2.14 is quite similar to the one determined from the simulated (210) plane of the D^A structure shown in **Figure 1c** inset (a/b = 2.25).

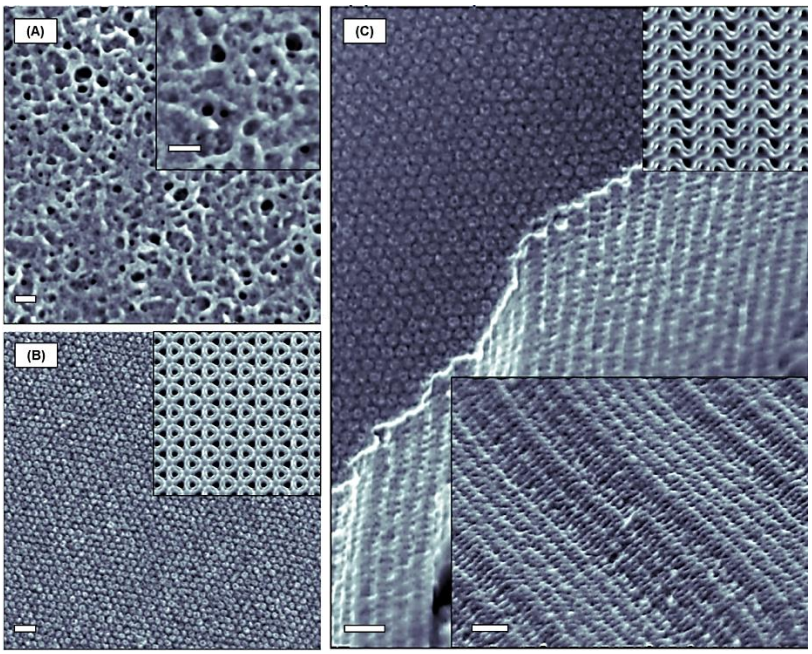

Figure 1: Top view SEM images of blended (25% wt.) PDMSB-*b*-PS-*b*-PMMA thick films manufactured by NIPS then exposed to a $CHCl_3$ vapor during different times: (a) 0h and (b, c) 3h. The disordered phase generated by NIPS on the top surface membrane is transformed into a highly-ordered D^A structure after the SVA treatment. Insets: Magnified SEM image showing (a) the dense regions formed by collapsed micelles after the NIPS process and (c) the D^A (210) pattern. Additionally, simulated cross-sectional images of the D^A structure cut parallel to (b) the (111) plane and (c) the (210) plane are presented. Scale bars: 100 nm.

In the regions of the thick film where the nanoring pattern is observed on the top surface layer, it turns out that the fracture propagations of the D^A structure occur preferentially along the (210) plane with a relative flatness inside the grains having a single orientation of the wavy stripe motif. This relative flatness is a good indication of a non-traumatic propagation of the fracture along the wavy stripe pattern having a PS matrix area fraction of ~57% (determined from a binarization of the simulated D^A (210) plane) and could explain the frequent observation of the D^A (210) plane. Importantly, this several micrometers thick D^A structure differs from the core-shell cylindrical morphology having a period of ~33 nm observed in thin film configuration after the SVA treatment (3h, $CHCl_3$).[22] This phenomenon is probably due to the fact that the 70 nm thick PDMSB-*b*-PS-*b*-PMMA layer blended with 25% wt. of PDMSB-*b*-PS chains is too thin to allow the formation of the D^A structure, as recently shown from sub-100 nm thick PDMSB-*b*-PS films for which a cylindrical phase was

observed for film thicknesses below the unit cell dimension of the double gyroid (DG, $Ia\bar{3}d$) structure.[27]

To demonstrate that the asymmetric structure of the blended (25 % wt.) thick films has not been destroyed during the SVA process, representative SEM images showing the lower, middle and upper regions of a solvent-annealed (3h, $CHCl_3$) PDMSB-*b*-PS-*b*-PMMA thick film are presented in **Figure 2**. The cross-sectional SEM view presented in **Figure 2a** indicates that the blended PDMSB-*b*-PS-*b*-PMMA thick film deposited on a silicon substrate has a thickness of ~24 μm. A nanostructured 3D-morphology of over 4 μm in thickness can be observed on the material top surface (see **Fig. 2b**) while a sponge-like substructure is clearly visible close to the Si substrate (see **Fig. 2c**). Although the disordered sponge-like morphology and the network structure are always separated from one another by a well-defined interface (see **Fig. S4**), some nanostructured grains drown in the sponge-like substructure can be seen in the middle of the blended PDMSB-*b*-PS-*b*-PMMA thick film, like those surrounded by the dashed red lines in **Figure 2d**. Importantly, in spite of the presence of a few nanostructured grains in the middle of the polymeric layer (revealing that the $CHCl_3$ vapor is able to deeply penetrate the material), the asymmetric structure of the blended material generated by NIPS is not disrupted during the post SVA process. This phenomenon is due to the fact that the sponge-like substructure must densify prior to be transformed into a well-ordered D^A phase, implying a strong collapse of the blended PDMSB-*b*-PS-*b*-PMMA thick film.

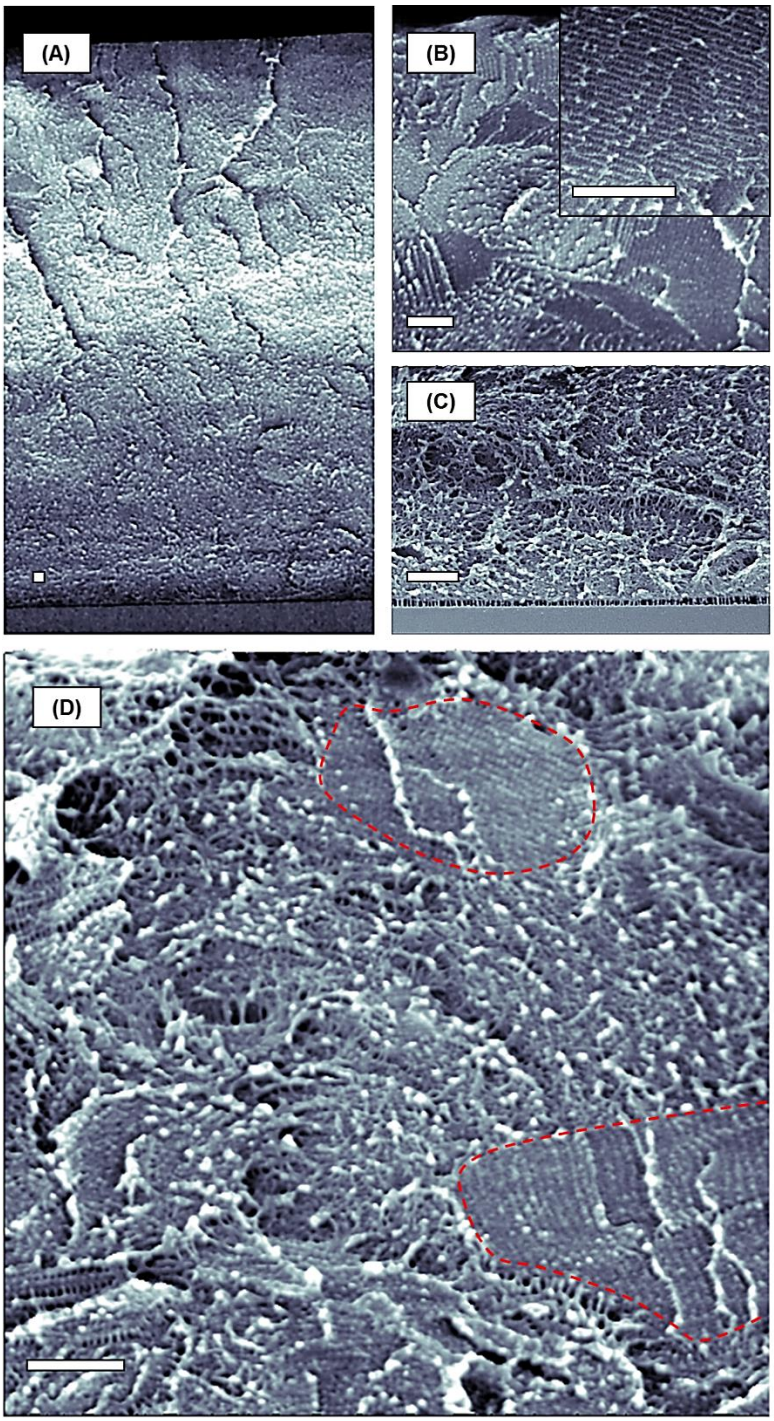

Figure 2: Cross-sectional SEM views of a blended (25% wt.) PDMSB-*b*-PS-*b*-PMMA thick film (t ~ 24 μm) generated by NIPS-SVA (3h, $CHCl_3$) showing: (a) the full material on a Si substrate, (b) the D^A structure formed within the material top layer, (c) the sponge-like substructure in the vicinity of the substrate, and (d) ordered D^A grains delimited by red dashed lines in the sponge-like substructure. Inset: Magnified SEM view showing the complex D^A structure. Scale bars: 0.5 μm.

For short time durations of the SVA process (t < 1h), the characteristic D^A (111) pattern is the most frequently observed on the free surface of the blended (25 % wt.) thick film. In

contrast, the (310) and (311) motifs of the D^A structure can be also encountered at the material-air interface when the time duration of the SVA process is increased. For instance, the atomic force microscopy (AFM) topographic and phase images taken from a blended (25 % wt.) PDMSB-*b*-PS-*b*-PMMA thick film exposed to a $CHCl_3$ vapor for 3h then treated by a CF_4/O_2 RIE plasma show the typical wavy stripe pattern of the D^A (310) plane oriented parallel to the air surface (see **Fig. 3a-b**).

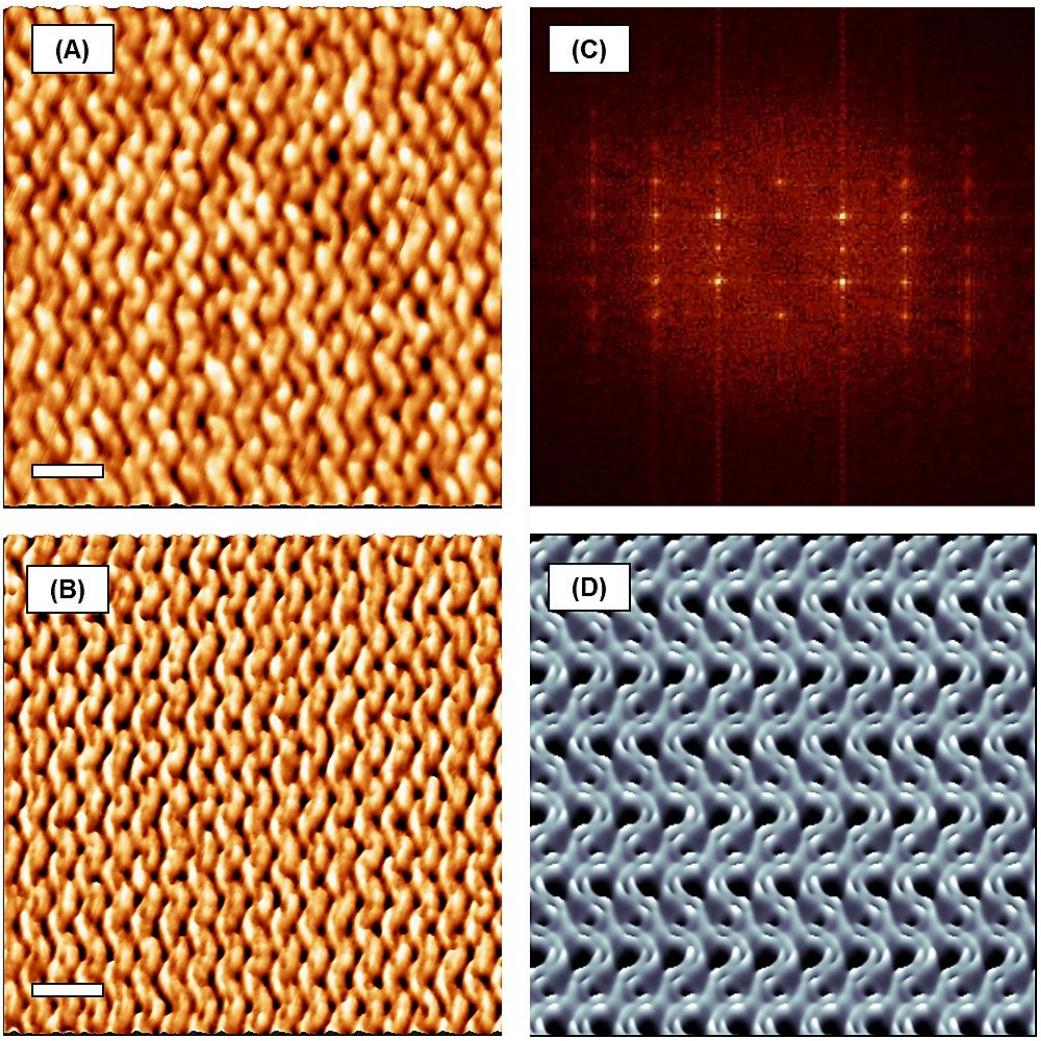

Figure 3: AFM (a) topographic and (b) phase views showing the D^A (310) plane oriented parallel to the air surface of a blended (25% wt.) PDMSB-*b*-PS-*b*-PMMA thick film generated by NIPS-SVA (3h, $CHCl_3$). (c) The 2D-FFT of the topographic image reveals that the wavy stripe pattern has *c*2*mm* symmetry. (d) Simulated cross-sectional image of the D^A structure cut parallel to the (310) plane. Scale bars: 100 nm.

The 2D fast Fourier Transform (FFT) of the AFM topographic image indicates that these wavy stripes are arranged into a centered rectangular array with the lattice parameters *a* =

74.1 nm and b = 40.7 nm (see **Fig. 3c**). The ratio a/b equal to 1.82 is very close to the one determined from the simulated D^A (310) plane presented in **Figure 3d** (a/b = 1.78). These wavy stripes are often confined inside macro-sized grains (> 1.5 μm^2) indicating a high crystalline quality of the alternating diamond morphology formed on the sponge-like substructure (see **Fig. S5**). Lozenge-like features arranged in an oblique lattice can be also observed on the material free surface as shown on the AFM topographic and phase views presented in **Figures 4a-b**.

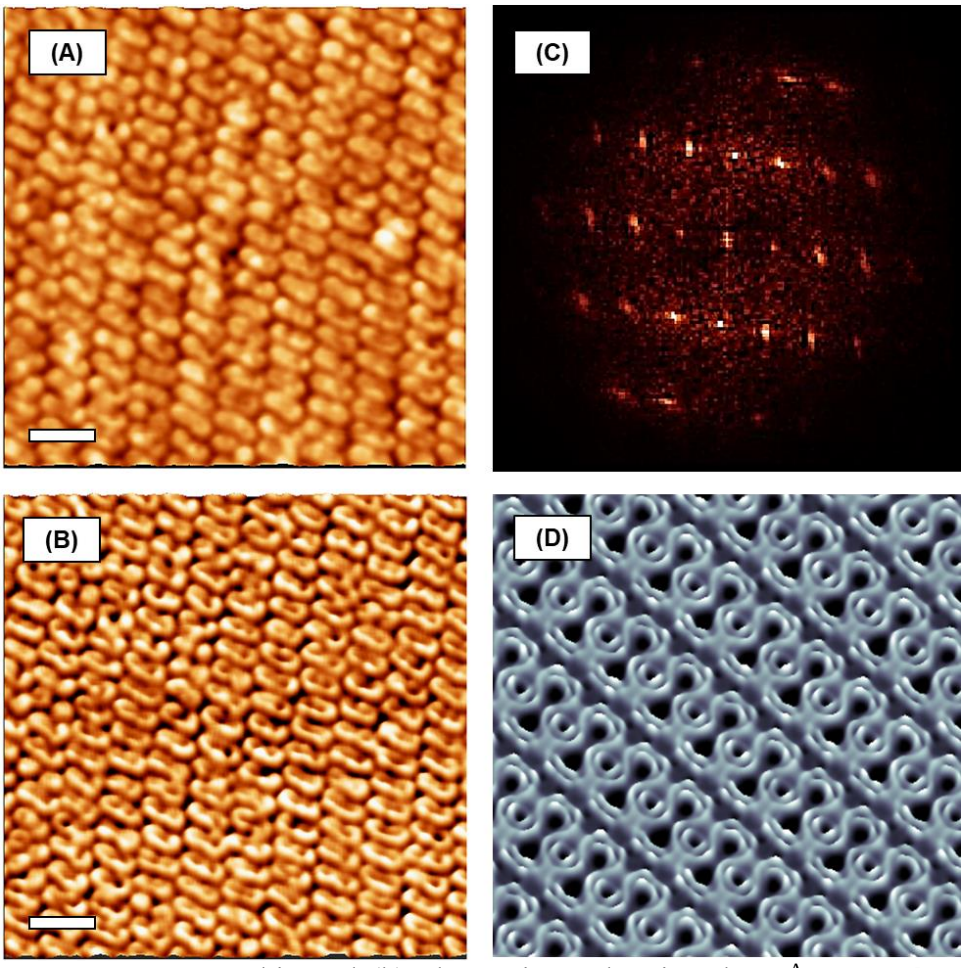

Figure 4: AFM (a) topographic and (b) phase views showing the D^A (311) plane oriented parallel to the air surface of a blended (25% wt.) PDMSB-*b*-PS-*b*-PMMA thick film generated by NIPS-SVA (3h, $CHCl_3$). (c) The 2D-FFT of the topographic image indicates that the lozenge-like features are arranged in an oblique lattice. (d) Simulated cross-sectional image of the D^A structure cut parallel to the (311) plane. Scale bars: 100 nm.

The 2D-FFT presented in **Figure 4c** indicates that this lozenge-like pattern (a = 64.5 nm, b = 36.3 nm and $\gamma \approx 100°$) has a ratio a/b equal to 1.77 which is quite similar to the one

determined from the simulated D^A (311) plane shown in **Figure 4d** ($a/b = \sqrt{3} \sim 1.73$). This lozenge-like motif can be also encountered inside large grains as shown on the AFM and SEM images presented in **Figure S6**. Note that other crystallographic planes of the D^A structure have been also observed within the material skin layer, which fully supports the formation of a well-developed network morphology during the SVA treatment (see **Fig. S7**).

Varying the amount of PDMDB-*b*-PS chains within the PDMSB-*b*-PS-*b*-PMMA material was revealed to be an efficient strategy to achieve another long-range ordered network structure on the material skin layer. Indeed, a perforated layer (PL) is produced on the top surface of solvent-annealed (3h, $CHCl_3$) PDMSB-*b*-PS-*b*-PMMA thick films blended with 35% wt. of PDMDB-*b*-PS chains as depicted in **Figure 5a**. For such morphology consisting of a PMMA-rich phase enclosed in PS lamellae and PDMSB lamellae perforated by PMMA/PS core-shell cylinders, two different patterns, corresponding to the (001) and (101) crystallographic planes of the PL structure, are commonly observed on the material skin layer. The top view SEM image presented in **Figure 5b** shows that the PL (001) pattern consists of PMMA/PS core-shell perforations ordered into a well-ordered hexagonal array having a period of ~27 nm. A hexagonal packing of perforations is commonly observed for the perforated layer structures in which the perforations are generally arranged into an AB or ABC stacking.[28–31] In contrast, a 27 nm period lamellar pattern without apparent perforations can be observed along the (101) plane (see **Fig. 5c**). The top view SEM images presented in **Figures 5d-e** show the layered structure inside the material skin layer at different magnifications. **Figure 5e** confirms the formation of a PL structure on the top surface layer since PS (bright) perforations are evident through the PDMSB (dark) lamellae. A perforated lamellar structure with core-shell perforations arranged into a rhombic array has been recently achieved on the skin layer of solvent-annealed ($CHCl_3$) PDMSB-*b*-PS-*b*-P2VP thick films.[32] For such PL structure having perforations stacked in ABAB… sequence, the (001) and (101)

planes were also the most frequently observed at the material-air interface. Unfortunately, here the stacking sequence of the PMMA/PS perforations is unclear from the SEM images.

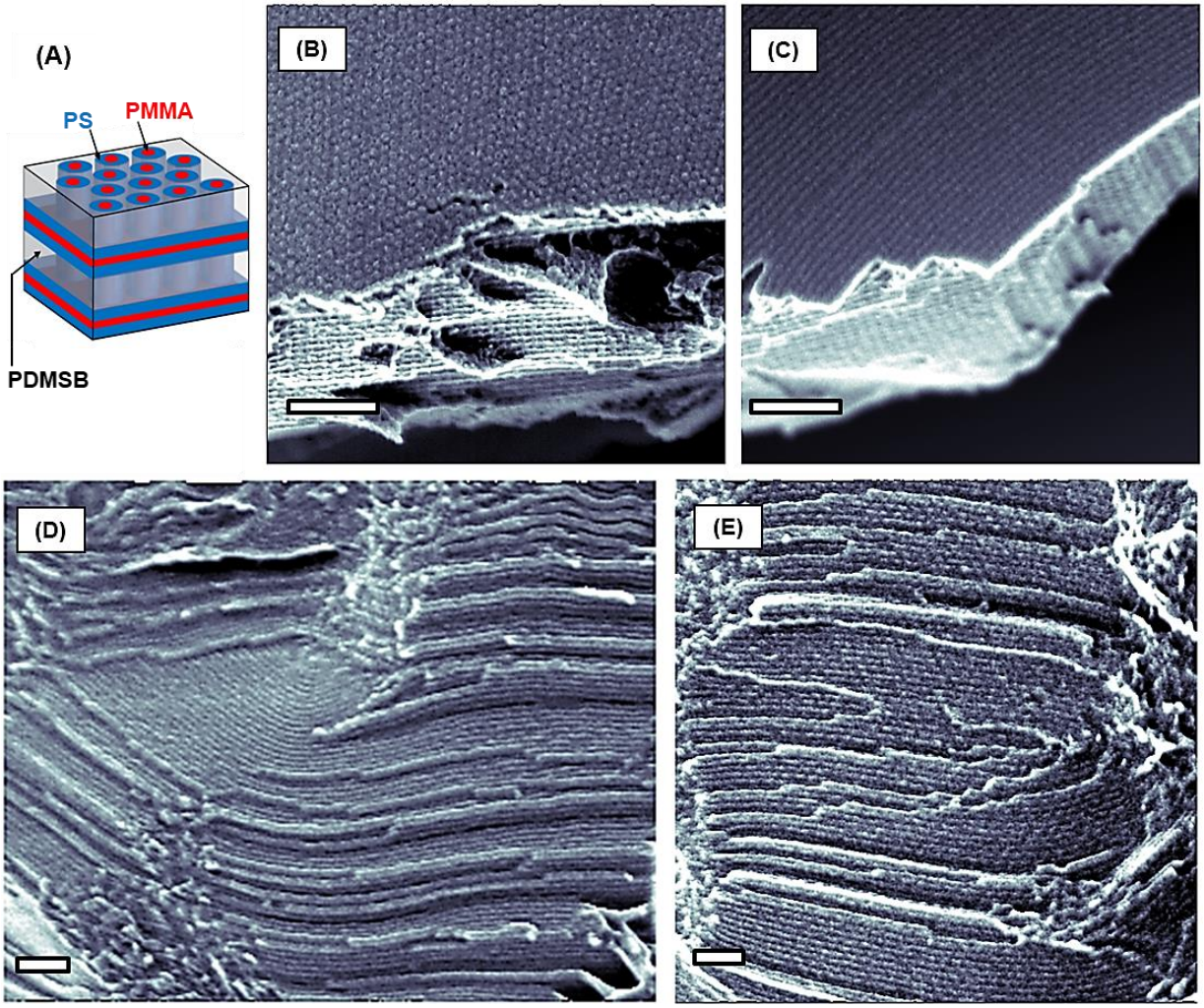

Figure 5: (a) Schematic representation of a bicontinuous PL structure having PMMA (red)/PS (blue) core-shell perforations. (b) and (c) Top view SEM images showing different PL planes oriented parallel to the air surface of a blended (35% wt.) PDMSB-*b*-PS-*b*-PMMA thick film generated by NIPS-SVA (3h, $CHCl_3$). (d) and (e) Top view SEM images, at different magnifications, showing the PL phase inside the material skin layer. Scale bars: 200 nm.

Conclusion

Bicontinuous network morphologies having an excellent long-range order were demonstrated on the skin layer of asymmetric and hydrophobic triblock terpolymer thick films manufactured by combining the conventional NIPS process with a SVA treatment used in advanced lithography application. Remarkably, an appealing triply periodic D^A nanostructure of unprecedented complexity is achieved for the first time on a sponge-like microstructure. We believe this simple and scalable NIPS-SVA method, enabling the formation of appealing network nanostructures which differs from the common cylindrical morphology generated by SNIPS, can be viewed as a first step in the process of preparing newly-designed membranes. Indeed, porous nanochannels are also mandatory to manufacture a permeable membrane. To avoid any additional challenging etching process to remove the PMMA nanopathways, pH-responsive P2VP-containing triblock terpolymer membranes, having either an open or closed state of the pores depending of the pH value, are currently being studied in our laboratory.

Methods

Fabrication of asymmetric PDMSB-*b*-PS-*b*-PMMA-based thick films: 24 μm thick PDMSB-*b*-PS-*b*-PMMA thick films were drawn onto (1.5 x 2 cm²) silicon substrates by using a tape casting technique from a 18 % wt. terpolymer solution in a mixture of 1,4-dioxane and tetrahydrofuran (DOX/THF: 80/20 by weight). To manufacture asymmetric materials with a sponge-like substructure, solvents were allowed to evaporate during 15s to form a dense skin layer, and then the thick films were immersed into a water bath for 10 min. to precipitate the PDMSB-*b*-PS-*b*-PMMA terpolymer. A SVA treatment was subsequently performed to transform the kinetically trapped morphology formed on the material top surface into a self-assembled nanostructure. As the neat PDMSB-*b*-PS-*b*-PMMA terpolymer self-assembles into

a core-shell cylindrical morphology when exposed to a $CHCl_3$ vapor, the terpolymer solution was blended with either 25% wt. or 35% wt. of PDMSB-*b*-PS chains to achieve different bicontinuous network structures.

Self-assembled PDMSB-*b*-PS-*b*-PMMA thick films: The self-assembly of unblended and blended PDMSB-*b*-PS-*b*-PMMA thick films was promoted by exposing the polymeric layers during different times to a continuous stream of $CHCl_3$ vapor produced by bubbling nitrogen gas through the liquid solvent as described previously.[33] This continuous flow system was used to control the $CHCl_3$ vapor pressure in the chamber having a lid made of quartz by dilution with a separate N_2 stream so that the solvent vapor consisted of 32 sccm $CHCl_3$ vapor and 8 sccm N_2 (total 40 sccm). As the in-situ measurement of the film thickness variation of an asymmetric thick film is not easy to achieve, the swelling ratio of a blended (25% wt.) PDMSB-*b*-PS-*b*-PMMA layer was estimated in thin configuration (initial thickness of ~95 nm), using a Filmetrics spectroscopic white light reflectometer apparatus (see **Fig. S8**). The blended layer, spin-coated (2 krpm) from a 2% wt. BCP solution in a mixture of tetrahydrofuran and propylene glycol monomethyl ether acetate (THF/PGMEA: 2/1), reached a plateau for a 70% thickness variation.

SEM and AFM Characterizations: Scanning electron microscopy (SEM, JEOL 7800) was used in Gentle Beam mode (GBSH) at an accelerating voltage of 1 kV to take PDMSB-*b*-PS-*b*-PMMA film images. Atomic force microscopy (AFM Dimension FastScan, Bruker) was used in tapping mode to characterize the surface morphology of blended and unblended PDMSB-*b*-PS-*b*-PMMA thick films. Silicon cantilevers (Fastscan-A) with a typical tip radius of ~5 nm were used. The resonance frequency of the cantilevers was about 1.25 kHz. Prior to SEM and AFM measurements, PDMSB-*b*-PS-*b*-PMMA thick films were etched with a fluorine-rich plasma treatment in PE-100 chamber (RIE, Plasma Etch) to remove partially and

preferentially the PDMSB and PMMA phases (plasma conditions: 40 W, 17 sccm CF_4 and 3 sccm O_2, 180 mTorr, and 45 s).

Small Angle X-ray Scattering (SAXS): SAXS experiments were performed on the D2AM French-CRG Beamline at the European Synchrotron Radiation Facility (ESRF) in Grenoble, France. A XPAD 2D pixel detector was used for recording the 2D scattering images, and a 2400 mm sample-to-detector distance was chosen. The energy of the X-ray beam was 11 keV. The 2D images were radially averaged around the center of the primary beam to obtain the isotropic SAXS intensity profiles. The scattering pattern from a specimen of silver behenate was used for the calibration of the wavevector scale of the scattering curves. Finally, the data were normalized to the intensity of the incident beam to correct for primary beam intensity fluctuations.

Acknowledgements

This work was performed within the framework of the Equipex ELORPrintTec ANR-10-EQPX-28-01 with the support of the ANR JCJC AFM_Ring project, grant ANR-18-CE09-00xx of the French Agence Nationale de la Recherche. The ESRF is acknowledged for allocating beamtime at the D2AM French Beamline for the SAXS experiments.

Associated Content

Supporting Information available: SEM images of a neat PDMSB-*b*-PS-*b*-PMMA thick film generated by NIPS-SVA (3h, $CHCl_3$); SAXS profile of a thermally-annealed (24h, 180°C) PDMSB-*b*-PS-*b*-PMMA sample; simulations for a cubic cell of the triply periodic bicontinuous D^A morphology and three different plane orientations; SEM images of a blended (25% wt.) PDMSB-*b*-PS-*b*-PMMA thick film generated by NIPS-SVA (3h, $CHCl_3$); AFM topographic view and its associated 2D-FFT corresponding to the D^A (310) plane of a blended (25% wt.) PDMSB-*b*-PS-*b*-PMMA thick film (3h, $CHCl_3$); AFM topographic views and a SEM image showing the D^A (311) plane oriented parallel to the air surface of a blended (25%

wt.) PDMSB-*b*-PS-*b*-PMMA thick film (3h, $CHCl_3$); panel of SEM images of a blended (25% wt.) PDMSB-*b*-PS-*b*-PMMA thick film; film thickness variation of a blended (25% wt.) PDMSB-*b*-PS-*b*-PMMA thin film plotted versus the swelling time in a $CHCl_3$ atmosphere.

References

(1) Mehta, A.; Zydney, A. L. Permeability and Selectivity Analysis for Ultrafiltration Membranes. *J. Memb. Sci.* **2005**, *249* (1–2), 245–249. https://doi.org/10.1016/J.MEMSCI.2004.09.040.

(2) Nunes, S. P. Block Copolymer Membranes for Aqueous Solution Applications. *Macromolecules*. American Chemical Society April 26, 2016, pp 2905–2916. https://doi.org/10.1021/acs.macromol.5b02579.

(3) Abetz, V. Isoporous Block Copolymer Membranes. *Macromol. Rapid Commun.* **2015**, *36* (1), 10–22. https://doi.org/10.1002/marc.201400556.

(4) Zhang, Y.; Sargent, J. L.; Boudouris, B. W.; Phillip, W. A. Nanoporous Membranes Generated from Self-Assembled Block Polymer Precursors: Quo Vadis ? *J. Appl. Polym. Sci.* **2015**, *132* (21), n/a-n/a. https://doi.org/10.1002/app.41683.

(5) Peinemann, K. V.; Abetz, V.; Simon, P. F. W. Asymmetric Superstructure Formed in a Block Copolymer via Phase Separation. *Nat. Mater.* **2007**, *6* (12), 992–996. https://doi.org/10.1038/nmat2038.

(6) Marques, D. S.; Vainio, U.; Chaparro, N. M.; Calo, V. M.; Bezahd, A. R.; Pitera, J. W.; Peinemann, K.-V.; Nunes, S. P. Self-Assembly in Casting Solutions of Block Copolymer Membranes. *Soft Matter* **2013**, *9* (23), 5557. https://doi.org/10.1039/c3sm27475f.

(7) Nunes, S. P.; Sougrat, R.; Hooghan, B.; Anjum, D. H.; Behzad, A. R.; Zhao, L.; Pradeep, N.; Pinnau, I.; Vainio, U.; Peinemann, K.-V. Ultraporous Films with Uniform Nanochannels by Block Copolymer Micelles Assembly. *Macromolecules* **2010**, *43*

(19), 8079–8085. https://doi.org/10.1021/ma101531k.

(8) Nunes, S. P.; Behzad, A. R.; Hooghan, B.; Sougrat, R.; Karunakaran, M.; Pradeep, N.; Vainio, U.; Peinemann, K.-V. Switchable pH-Responsive Polymeric Membranes Prepared *via* Block Copolymer Micelle Assembly. *ACS Nano* **2011**, *5* (5), 3516–3522. https://doi.org/10.1021/nn200484v.

(9) Phillip, W. A.; Mika Dorin, R.; Werner, J.; Hoek, E. M. V.; Wiesner, U.; Elimelech, M. Tuning Structure and Properties of Graded Triblock Terpolymer-Based Mesoporous and Hybrid Films. *Nano Lett.* **2011**, *11* (7), 2892–2900. https://doi.org/10.1021/nl2013554.

(10) Qiu, X.; Yu, H.; Karunakaran, M.; Pradeep, N.; Nunes, S. P.; Peinemann, K. V. Selective Separation of Similarly Sized Proteins with Tunable Nanoporous Block Copolymer Membranes. *ACS Nano* **2013**, *7* (1), 768–776. https://doi.org/10.1021/nn305073e.

(11) Gu, Y.; Wiesner, U. Tailoring Pore Size of Graded Mesoporous Block Copolymer Membranes: Moving from Ultrafiltration toward Nanofiltration. *Macromolecules* **2015**, *48* (17), 6153–6159. https://doi.org/10.1021/acs.macromol.5b01296.

(12) Hahn, J.; Filiz, V.; Rangou, S.; Clodt, J.; Jung, A.; Buhr, K.; Abetz, C.; Abetz, V. Structure Formation of Integral-Asymmetric Membranes of Polystyrene-Block-Poly(ethylene Oxide). *J. Polym. Sci. Part B Polym. Phys.* **2013**, *51* (4), 281–290. https://doi.org/10.1002/polb.23209.

(13) Saleem, S.; Rangou, S.; Abetz, C.; Lademann, B.; Filiz, V.; Abetz, V. Block Copolymer Membranes from Polystyrene-B-Poly(solketal Methacrylate) (PS-b-PSMA) and Amphiphilic Polystyrene-b-Poly(glyceryl Methacrylate) (PS-B-PGMA). *Polymers (Basel).* **2017**, *9* (6). https://doi.org/10.3390/polym9060216.

(14) Schöttner, S.; Schaffrath, H.-J.; Gallei, M. Poly(2-Hydroxyethyl Methacrylate)-Based

Amphiphilic Block Copolymers for High Water Flux Membranes and Ceramic Templates. *Macromolecules* **2016**, *49* (19), 7286–7295. https://doi.org/10.1021/acs.macromol.6b01803.

(15) Clodt, J. I.; Filiz, V.; Rangou, S.; Buhr, K.; Abetz, C.; Höche, D.; Hahn, J.; Jung, A.; Abetz, V. Double Stimuli-Responsive Isoporous Membranes via Post-Modification of Ph-Sensitive Self-Assembled Diblock Copolymer Membranes. *Adv. Funct. Mater.* **2013**, *23* (6), 731–738. https://doi.org/10.1002/adfm.201202015.

(16) Schacher, F.; Ulbricht, M.; Müller, A. H. E. Self-Supporting, Double Stimuli-Responsive Porous Membranes from Polystyrene-Block-poly(N,N-Dimethylaminoethyl Methacrylate) Diblock Copolymers. *Adv. Funct. Mater.* **2009**, *19* (7), 1040–1045. https://doi.org/10.1002/adfm.200801457.

(17) Jung, A.; Filiz, V.; Rangou, S.; Buhr, K.; Merten, P.; Hahn, J.; Clodt, J.; Abetz, C.; Abetz, V. Formation of Integral Asymmetric Membranes of AB Diblock and ABC Triblock Copolymers by Phase Inversion. *Macromol. Rapid Commun.* **2013**, *34* (7), 610–615. https://doi.org/10.1002/marc.201200770.

(18) Ju, X.-J.; Liu, Z.; Chu, L.-Y.; Xie, R.; Wang, W. Stimuli-Responsive Smart Gating Membraneskarunakaran. *Chem. Soc. Rev.* **2015**, *45* (3), 460–475. https://doi.org/10.1039/c5cs00692a.

(19) Yu, H.; Qiu, X.; Moreno, N.; Ma, Z.; Calo, V. M.; Nunes, S. P.; Peinemann, K. Self-Assembled Asymmetric Block Copolymer Membranes : Bridging the Gap from Ultra- to Nanofiltration Angewandte. **2015**, 13937–13941. https://doi.org/10.1002/anie.201505663.

(20) Karunakaran, M.; Shevate, R.; Peinemann, K. V. Nanostructured Double Hydrophobic Poly(styrene-B-Methyl Methacrylate) Block Copolymer Membrane Manufactured via a Phase Inversion Technique. *RSC Adv.* **2016**, *6* (35), 29064–29071.

https://doi.org/10.1039/c6ra02313d.

(21) Chisca, S.; Musteata, V.-E.; Sougrat, R.; Behzad, A. R.; Nunes, S. P. Artificial 3D Hierarchical and Isotropic Porous Polymeric Materials. *Sci. Adv.* **2018**, *4* (5), eaat0713. https://doi.org/10.1126/sciadv.aat0713.

(22) Aissou, K.; Mumtaz, M.; Marcasuzaa, P.; Brochon, C.; Cloutet, E.; Fleury, G.; Hadziioannou, G. Highly Ordered Nanoring Arrays Formed by Templated Si-Containing Triblock Terpolymer Thin Films. *Small* **2017**, *13* (12). https://doi.org/10.1002/smll.201603184.

(23) Bates, F. S. N Etwork Phases in Block Copolymer Melts. **2005**, *30* (JULY), 525–532.

(24) Aissou, K.; Mumtaz, M.; Fleury, G.; Portale, G.; Navarro, C.; Cloutet, E.; Brochon, C.; Ross, C. A.; Hadziioannou, G. Sub-10 Nm Features Obtained from Directed Self-Assembly of Semicrystalline Polycarbosilane-Based Block Copolymer Thin Films. *Adv. Mater.* **2015**, *27* (2). https://doi.org/10.1002/adma.201404077.

(25) Lee, S.; Cheng, L.-C.; Yager, K. G.; Mumtaz, M.; Aissou, K.; Ross, C. A. *In Situ* Study of ABC Triblock Terpolymer Self-Assembly under Solvent Vapor Annealing. *Macromolecules* **2019**, acs.macromol.8b02273. https://doi.org/10.1021/acs.macromol.8b02273.

(26) Asai, Y.; Suzuki, J.; Aoyama, Y.; Nishioka, H.; Takano, A.; Matsushita, Y. Tricontinuous Double Diamond Network Structure from Binary Blends of ABC Triblock Terpolymers. *Macromolecules* **2017**, *50* (14), 5402–5411. https://doi.org/10.1021/acs.macromol.7b00403.

(27) Aissou, K.; Mumtaz, M.; Portale, G.; Brochon, C.; Cloutet, E.; Fleury, G.; Hadziioannou, G. Templated Sub-100-nm-Thick Double-Gyroid Structure from Si-Containing Block Copolymer Thin Films. *Small* **2017**, *13* (20). https://doi.org/10.1002/smll.201603777.

(28) Hamley, I. W.; Koppi, K. A.; Rosedale, J. H.; Bates, F. S.; Almdal, K.; Mortensen, K. Hexagonal Mesophases between Lamellae and Cylinders in a Diblock Copolymer Melt. *Macromolecules* **1993**, *26* (22), 5959–5970. https://doi.org/10.1021/ma00074a018.

(29) Hajduk, D. A.; Takenouchi, H.; Hillmyer, M. A.; Bates, F. S.; Vigild, M. E.; Almdal, K. Stability of the Perforated Layer (PL) Phase in Diblock Copolymer Melts. *Macromolecules* **1997**, *30* (13), 3788–3795. https://doi.org/10.1021/ma961673y.

(30) Zhu, L.; Huang, P.; Cheng, S.; Ge, Q.; Quirk, R.; Thomas, E.; Lotz, B.; Wittmann, J.-C.; Hsiao, B.; Yeh, F.; Liu, L. Dislocation-Controlled Perforated Layer Phase in a PEO- *b*-PS Diblock Copolymer. *Phys. Rev. Lett.* **2001**, *86* (26), 6030–6033. https://doi.org/10.1103/PhysRevLett.86.6030.

(31) Ji, N.; Tang, P.; Qiu, F.; Shi, A.-C. C. Kinetic Pathways of Lamellae to Gyroid Transition in Weakly Segregated Diblock Copolymers. *Macromolecules* **2015**, *48* (23), 8681–8693. https://doi.org/10.1021/acs.macromol.5b02023.

(32) Aissou, K.; Mumtaz, M.; Bouzit, H.; Pécastaings, G.; Portale, G.; Fleury, G.; Hadziioannou, G. Bicontinuous Network Nanostructure with Tunable Thickness Formed on Asymmetric Triblock Terpolymer Thick Films. *Macromolecules* **2019**, https://doi.org/10.1021/ acs.macromol.9b00572.

(33) Gotrik, K. W.; Hannon, A. F.; Son, J. G.; Keller, B.; Alexander-Katz, A.; Ross, C. A. Morphology Control in Block Copolymer Films Using Mixed Solvent Vapors. *ACS Nano* **2012**, *6* (9), 8052–8059. https://doi.org/10.1021/nn302641z.

Use for table of content only